


ORIGINAL ARTICLE

Spectral signatures in the UV range can be combined with secondary plant metabolites by deep learning to characterize barley–powdery mildew interaction

Anna Brugger¹  | Patrick Schramowski² | Stefan Paulus³ | Ulrike Steiner¹ | Kristian Kersting⁴ | Anne-Katrin Mahlein³

¹University of Bonn, Institute for Crop Science and Resource Conservation (INRES)—Plant Pathology, Bonn, Germany

²Computer Science Department, Technical University Darmstadt, Darmstadt, Germany

³Institute of Sugar Beet Research, Göttingen, Germany

⁴Computer Science Department and Centre for Cognitive Science, Technical University Darmstadt, Darmstadt, Germany

Correspondence

Anna Brugger, University of Bonn, Institute for Crop Science and Resource Conservation (INRES)—Plant Pathology, Nussallee 9, 53115 Bonn, Germany. Email: abrugger@uni-bonn.de

Funding information

German Federal Ministry of Food and Agriculture, Grant/Award Number: FKZ 2818204715; Deutsche Forschungsgemeinschaft, Grant/Award Number: EXC 2070 – 390732324

Abstract

In recent studies, the potential of hyperspectral sensors for the analysis of plant–pathogen interactions was expanded to the ultraviolet range (UV; 200–380 nm) to monitor stress processes in plants. A hyperspectral imaging set-up was established to highlight the influence of early plant–pathogen interactions on secondary plant metabolites. In this study, the plant–pathogen interactions of three different barley lines inoculated with *Blumeria graminis* f. sp. *hordei* (Bgh, powdery mildew) were investigated. One susceptible genotype (cv. Ingrid, wild type) and two resistant genotypes (Pallas 01, *Mla1*- and *Mla12*-based resistance and Pallas 22, *mlo5*-based resistance) were used. During the first 5 days after inoculation (dai) the plant reflectance patterns were recorded and plant metabolites relevant in host–pathogen interactions were studied in parallel. Hyperspectral measurements in the UV range revealed that a differentiation between barley genotypes inoculated with Bgh is possible, and distinct reflectance patterns were recorded for each genotype. The extracted and analysed pigments and flavonoids correlated with the spectral data recorded. A classification of noninoculated and inoculated samples with deep learning revealed that a high performance can be achieved with self-attention networks. The subsequent feature importance identified wavelengths as the most important for the classification, and these were linked to pigments and flavonoids. Hyperspectral imaging in the UV range allows the characterization of different resistance reactions, can be linked to changes in secondary plant metabolites, and has the advantage of being a non-invasive method. It therefore enables a greater understanding of plant reactions to biotic stress, as well as resistance reactions.

KEY WORDS

Blumeria graminis f. sp. *hordei*, deep learning, *Hordeum vulgare*, hyperspectral imaging, secondary plant metabolites, UV range

This is an open access article under the terms of the Creative Commons Attribution License, which permits use, distribution and reproduction in any medium, provided the original work is properly cited.

© 2021 The Authors. Plant Pathology published by John Wiley & Sons Ltd on behalf of British Society for Plant Pathology.

1 | INTRODUCTION

In recent plant phenotyping studies, the ultraviolet range (UV; 200–380 nm) has been used for the first time to record reflectance properties of plants by hyperspectral imaging (Brugger et al., 2019). An extension of spectral measurements to this range enables the consideration of secondary plant substances such as flavonoids with an absorption maximum in the UV range (Table 1; Taniguchi & Lindsey, 2018). These secondary plant substances are produced in response to abiotic or biotic stress. Therefore, hyperspectral measurements in the UV range can lead to more detailed knowledge about plant responses to stress factors.

The obligate biotrophic ascomycete *Blumeria graminis* f. sp. *hordei* (Bgh) causes powdery mildew on barley and influences the secondary plant metabolism. After infection with Bgh, barley leaves show typical white pustules which develop to form conidia which are dispersed by wind. The primary and secondary germ tubes develop within the first 4 h of infection, and the penetration peg is developed after 15 h. The first fungal colonies are visible to the naked eye 3–5 days after infection (dai; Both et al., 2005). An infection with Bgh leads to changes in plant metabolism and secondary plant metabolites such as flavonoids, which are polyphenolic secondary plant metabolites. Within the flavonoid group, anthocyanins and flavonols have various tasks such as visual signals, auxin transport, and resistance against plant pathogens (Petrussa et al., 2013). High contents of flavonoids such as kaempferol and pelargonidin have been found in plants exposed to high levels of UV radiation (Monici et al., 1993). Anthocyanins protect chloroplasts from UV radiation but can also scavenge reactive oxygen species (Neill & Gould, 2003). High levels have been found in primary leaves of barley, where they are stored in the epidermis. Their high absorptive properties of UV light means that they can also be found in the mesophyll (Liu et al., 1995).

The flavone chrysin, present in different cereals (Liu et al., 2010), is often used to quantify flavonoids with spectrophotometric detection because their absorption maxima are at 240–290 nm as well as 310–370 nm (Mierziak et al., 2014). Flavonoids can not

only be synthesized by plants as a response to stress, but can also be produced before stress occurs and stored at important sites to play a direct role in defence mechanisms (Treutter, 2006). Studies have proposed that they are stored in epidermal cells and released into infected tissue, where they may be involved in hypersensitive responses (HR; Beckman, 2000). In addition, degradation of plant pigments such as carotenoids and chlorophyll *a* and *b*, with an absorption maximum at 400–500 nm (Taniguchi & Lindsey, 2018), can be linked to a changing photosynthetic activity due to compatible and incompatible interactions (Brugger et al., 2018). Other plant compounds are affected by infection of barley with Bgh as well as flavonoids; for example, genotypes susceptible to Bgh showed a reduced electron transport capacity due to a degraded photosystem II, which results in a loss of chlorophyll during infection development (Scholes et al., 1994).

Resistance breeding is a major protection strategy against Bgh infections in barley. The cultivar Ingrid (wild type, WT) is susceptible to infections, while cv. Pallas has two isogenic lines O1 and 22, which are resistant and show no typical symptoms of a powdery mildew infection. Pallas O1 has a race specific resistance and possesses the resistance genes mildew loci *Mla1* and *Mla12*, which cause a HR after recognizing specific Bgh avirulence genes (Schulze-Lefert & Vogel, 2000). The near-isogenic line Pallas 22 contains a dysfunction in the *mlo5* gene and has a broad-spectrum papilla-based resistance against Bgh (Kølster et al., 1986). A papilla or cell wall apposition (CWA) is quickly developed below the penetration point of the pathogen and prevents further infection development. CWAs contain phenols, belonging to the secondary plant metabolite group of flavonoids (Jørgensen, 1992).

The susceptible and resistant barley–Bgh interaction has previously been studied with hyperspectral imaging in the visible (400–700 nm) and near infrared (700–1000 nm) range, with emphasis on reflectance and transmission data (Kuska et al., 2015; Thomas et al., 2016). Reflection measurements enabled an early detection of infection two days before colonies became visible to the naked eye (Thomas et al., 2016). In addition, the genotypes were differentiated

TABLE 1 List of important secondary metabolites with an absorption maximum in the UV-range

Secondary plant metabolite	Absorption source maxima (nm)	Reference
Acridone	398	Reiser et al., (1972)
Anthocyanin	270–290	Woodall and Stewart (1998)
Carotenoids	400–500	Lichtenthaler and Buschmann (2001)
Chlorophyll <i>a</i>	428	Seely and Jensen (1965)
Chlorophyll <i>b</i>	453	Seely and Jensen (1965)
Coumarin	311	Abu-Eittah and El-Tawil (1985)
Flavonoids	240–290, 310–370	Mierziak et al., (2014)
Hydroquinone	295	Stalin et al., (2005)
Phenol	271	Stalin et al., (2005)
Quinoline	313	Snyder and Testa (1984)

according to their susceptibility to Bgh (Kuska et al., 2015) and this data was combined with microscopic observations (Kuska et al., 2017) and results from invertase analysis (Kuska et al., 2018). At present, there is no research available that links the secondary metabolism of the plant with spectral changes of wavelengths. The genotypes used in this study serve as a model to prove the usability of the UV range to describe phytopathogens and their effects on host plants.

Three hypotheses were investigated in this study: (a) an infection with Bgh affects the secondary plant metabolites, (b) the changes in secondary metabolism can be detected by noninvasive hyperspectral imaging, and (c) the relevant wavelengths can be narrowed down by combining the recorded hyperspectral data with deep learning algorithms (Figure 1). The last point is particularly important to be able to limit future investigations to the relevant wavelengths of the UV range in a targeted and cost-saving manner.

2 | MATERIALS AND METHODS

2.1 | Plant cultivation and pathogen inoculation

The barley lines cv. Ingrid wild type (WT), Pallas 01 (*Mla12*), and Pallas 22 (*mlo5*) were grown in a greenhouse environment in plastic pots (5 × 5 cm) on commercial substrate (Topfsubstrat 1.5, Balster Erdenwerk GmbH) and watered, as necessary. After 10 days when

reaching growth stage 11 (Witzenberger et al., 1989) the primary leaves were cut at 10 cm and place on 10 g/L phytotagar (Duchefa Biochemie B.V.) containing 0.34 mM benzimidazole (Kuska et al., 2015). For each genotype, 10 leaves were kept untreated as a control group, while eight technical replications with five leaves each were inoculated with fresh spores of Bgh isolate A6. The agar plates were sealed and incubated at 19°C in a controlled environment with 1,100 cd/m² illuminance and a photoperiod of 16 h per day.

2.2 | Extraction of secondary plant metabolites

For the extraction of secondary plant metabolites, samples of inoculated and noninoculated barley leaves of all three genotypes were collected 1 to 5 dai and kept in the freezer at -80°C until analysis. The extraction was carried out for six biological replications.

2.3 | Chlorophyll and carotenoid extraction

Chlorophyll and carotenoid extraction was performed according to Scholes et al., (1994). Frozen leaf samples with 0.5 M HClO₄ were ground in liquid nitrogen to a fine powder. Subsequently, 0.5 g per sample was transferred into a tube stored on ice and 1.5 ml of 80% acetone was added. The samples were kept for 3 hr on ice in the dark and mixed every 20 min. The samples were then centrifuged at 4°C at 21,000 × g for 20 min and the absorption of the extract was measured at 470, 645, and 663 nm. The concentration of chlorophyll and carotenoid was calculated according to Hiscox and Israelstam (1979).

2.4 | Total flavonoid extraction

Total flavonoid extraction was performed according to Mihai et al., (2010). Frozen leaf samples were ground in liquid nitrogen to a fine powder and extracted with 96% ethanol. For this, 1 g of each sample was mixed with 30 ml ethanol and kept overnight with constant stirring. Samples were then filtered on qualitative filter paper three times before the volume was made up to 100 ml for an initial extract concentration of 1%. Of this extract, 3 ml were mixed with 1 ml 2.5% ZrOCl₂ and 21 ml methanol were added. After 30 min, the absorption was measured at 288 nm against a control solution consisting of methanol. A calibration curve was established using chrysin. For this, a stock solution with 0.1 mg/ml was prepared and aliquots of 0.25, 0.5, 1, 1.5, and 2 ml were used. The measured absorbance was plotted against the concentration to establish the calibration curve.

2.5 | Hyperspectral image acquisition and data preprocessing

Spectral reflectance was recorded with a hyperspectral imaging line scanner in the UV range according to Brugger et al., (2019),

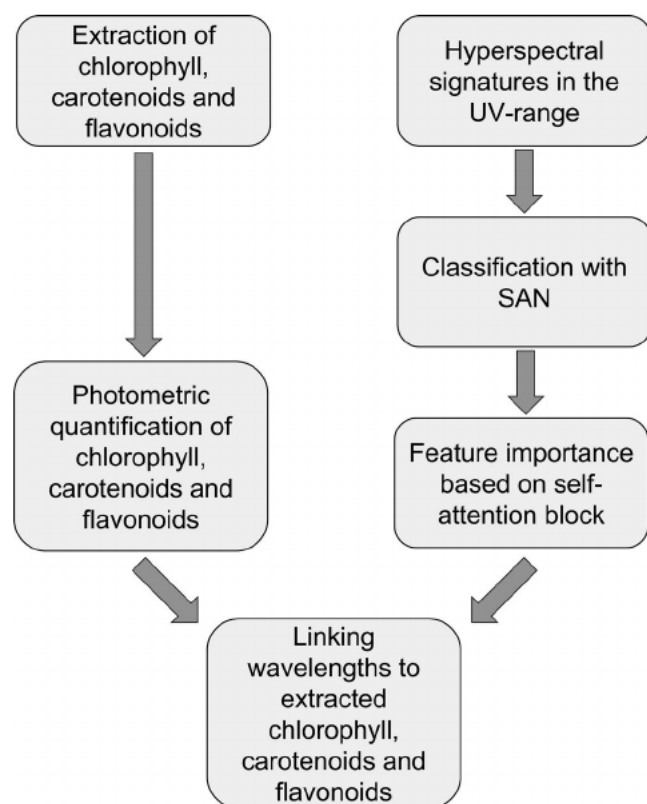


FIGURE 1 Workflow to investigate whether spectral images in the UV range can be linked with changes in secondary plant metabolites

with an exposure time of 800 ms, a frame rate of 0.4 frames/s, and a linear axis speed of 0.3 mm/s. The reflectance was measured daily from 1 to 5 dai. The relative reflectance was calculated using the software Hyperspec III (Headwall Photonics) and for this purpose, a white reference image of 95% barium sulphate and a dark current image were recorded. Data were then analysed with the software ENVI 5.5 (Exelis Visual Information Solutions). A manually selected 7,500 pixel sample from each image was used to calculate the average reflectance. The selected pixels covered the entire barley leaf. A Savitzky-Golay filter with a window size of 7 and a 3rd degree polynomial was used to preprocess the data. The Savitzky-Golay filter and the corresponding parameters were selected to reduce the signal noise while preserving the properties of the signal distribution (Madden, 1978). Figures were generated with SigmaPlot 14 (Systat Software). RGB visualization was performed 1 to 5 dai.

2.6 | Experimental setup of sample classification

The superpixels from the data were used as input for the (deep) learning algorithms to classify the measurements into noninoculated and inoculated samples. A superpixel is defined as the average of $P \times P$ neighbouring pixels. A spatial area with $p = 7$ was selected so that it was likely to contain symptoms. The computed areas were nonoverlapping. The data were split into two different sets for training and testing. The test set contained 20% of the data and the results were cross-validated so that five different models were trained and evaluated for each classification task.

2.7 | Determination of relevant features with self-attention classification networks

To determine the meaning of the characteristics of the hyperspectral data, the neural network architecture self-attention networks (SAN; Skrlj et al., 2020) were used. SANs are motivated by recent advances in natural language processing, for example, through the language model BERT (Devlin et al., 2018) with the transformer network architecture (Vaswani et al., 2017). A key feature of these architectures is the so-called self-attention mechanism. Skrlj et al. (2020) have shown that self-attention can also be used to identify the relevant features per data point and that doing so can result in better classification accuracy than previous methods. The network architecture can be described as follows:

$$SAN = \sigma(W_2 \times (a(W_{|F|} \Omega(X) + b_{l_1}))) + b_{l_2} \quad (1)$$

$$\Omega(X) = \frac{1}{k} \oplus \left[\underbrace{x \otimes \text{softmax}(W_{att}^k X + b_{att}^k)}_{\text{Attention}} \right] \quad (2)$$

where K is the number of parallel self-attention blocks, X is the input, and W and b are learnable parameters of the network. The functions a and σ are activation functions. In this case a is a SELU (Klambauer et al., 2017) and σ softmax function. The symbol \otimes corresponds to the Hadamard product while the symbol \oplus refers to the Hadamard sum formation over individual blocks. The first neural network layer is used especially for maintaining the connection with the input features F . The input vectors are first used as input for the softmax-activated layer, whose neurons match with the number of features F . The softmax function is defined as following:

$$\text{softmax}(v_{ji}) = \frac{\exp(v_{ji})}{\sum_{j=1}^F \exp(v_j)} \quad (3)$$

The self-attention mechanism effectively creates a sparsely populated input area and only emphasizes relevant features for solving the task at hand (e.g., language comprehension). In this way, the self-attention mechanism is often used to, for example, more accurately learn the relationships between words (Skrlj et al., 2020). In the present paper, SAN is used for the classification of individual signatures (pixels) or combined signatures (superpixels) of hyperspectral data in the UV range, classified between healthy and inoculated samples of different genotypes. The networks' self-attention mechanism weights the input features and uses the weighted output for the neural classification network. Two self-awareness heads and a neural classification network with 64 latent neurons were selected for the self-attention networks (SAN). The final feature importance is calculated by averaging the feature importance of the two heads:

$$\text{Feature Importance} = \frac{1}{k} \oplus [\text{softmax}(W_{att}^k X + b_{att}^k)] \quad (4)$$

where X is the evaluated set of inputs and in this case $k = 2$. The training setup of Skrlj et al. (2020) was followed and the network was trained with the commonly used Adam optimization algorithm (Kingma & Ba, 2014). However, the described batch size seemed to be very low. To achieve a more stable training, it was increased to 128 samples. A learning rate of 0.001 was used and it was gradually reduced during training. In a preprocessing step, the first wavelengths were removed, because they were characterized by increased noise, resulting in an input wavelength range from 260.232 to 501.219 nm.

2.8 | Gradient boosting as classification method

The framework XGBoost (Chen & Guestrin, 2016) was used to implement the baseline gradient boosting (GB) classifier. The machine learning technique GB can be used for classification as well as regression problems and generates a predictive model in the form of an ensemble of weak predictive models, usually decision trees. As in other boosting methods, the model is built up stage-wise. The hyperparameters to optimize the GB model were chosen empirically. The reported results were achieved using a maximum tree depth of

6 and a learning rate of 0.3. Further, a L2 regularization was used with the weight $\lambda = 1$.

3 | RESULTS

3.1 | Impact of compatible and incompatible barley Bgh interactions on pigment and flavonoid concentration

Chlorophyll, carotenoid, and total flavonoid content showed changes depending on the resistance of the host plant. The total chlorophyll content of all genotypes decreased between 1 and 5 dai. In WT leaves there was a strong decrease from 5.2 to 3.1 $\mu\text{g/g}$ between 1 and 5 dai, whereas in *mlo5* leaves, there was only a slight decrease from 5.7 to 5.1 $\mu\text{g/g}$. (Figure 2). The carotenoid extraction revealed a similar pattern for WT leaves. The highest value was measured 1 dai and decreased by 76% 5 dai. *Mla1* leaves demonstrated a strong decrease from 2.2 $\mu\text{g/g}$ 1 dai to 1.4 $\mu\text{g/g}$ 3 dai, but exhibited no further decrease 5 dai. Inoculated *mlo5* leaves were represented by a constant carotenoid concentration. The flavonoid content of WT leaves decreased from 49% 1 dai to 40% 5 dai. *Mla1* leaves displayed a decrease of 12% from 1 to 3 dai but stayed constant 5 dai. *mlo5* leaves demonstrated an increase from 47% 1 dai to 59% 3 dai, and remained constant 5 dai.

3.2 | Phenotypic development of Bgh on barley leaves

The phenotypic development of noninoculated and Bgh-inoculated barley leaves of Ingrid and the near-isogenic lines Pallas 01 and Pallas 22 were visualized with RGB images (Figures 3 and 4). Noninoculated leaves of all three genotypes remained healthy and

showed no visible disease symptoms (Figure 4). Inoculated leaves of the susceptible WT exhibited senescence starting 3 dai and typical white pustules 4 dai. These pustules were unevenly distributed on the leaves and covered approximately 60% of the leaf area 5 dai. Chlorotic tissue was seen in the area around powdery mildew pustules. Resistant *Mla1* and *mlo5* leaves showed no typical symptoms of infection with Bgh. Starting 4 dai, *Mla1* leaves displayed HR, visible under the microscope as necrotic brown spots heterogeneously distributed over the leaves.

3.3 | Spectral signatures of inoculated and noninoculated barley lines

Spectral signatures enabled the differentiation between different host-pathogen interactions. Distinct peaks between 250 and 312 nm, for example, at 258 nm, 266 nm, or 271 nm, characterized the reflectance of each sample. Additional peaks were visible between 410 and 440 nm, for example, at 421, 423, or 439 nm (Figure 5). The highest reflectance of each measurement was recorded at 254 nm at a value of 0.4%. Noninoculated barley leaves demonstrated constant spectral signatures, with a decrease in reflectance from 0.4% at 255 nm to 0.15% at 450 nm. The reflectance remained constant during the entire time-series measurements from 1 to 5 dai. Inoculated susceptible WT leaves presented a decreasing reflectance at 254 nm from 0.42% at 1 dai to 0.38% at 3 dai, before reaching the highest value of 0.47% at 4 dai. This decrease in reflectance was continuous from 250 to 400 nm, whilst the reflectance of all measurements was similar between 418 and 430 nm, at 0.14%. The smallest reflectance at 500 nm was 0.12% at 1 dai and increased to 0.145% at 5 dai. The race-specific resistant genotype *Mla1* exhibited the smallest reflectance at 254 nm 1 dai, which increased to its highest value of 0.48% 4 dai, and then decreased to 0.47% 5 dai. Similar to the susceptible WT, the reflectance of all

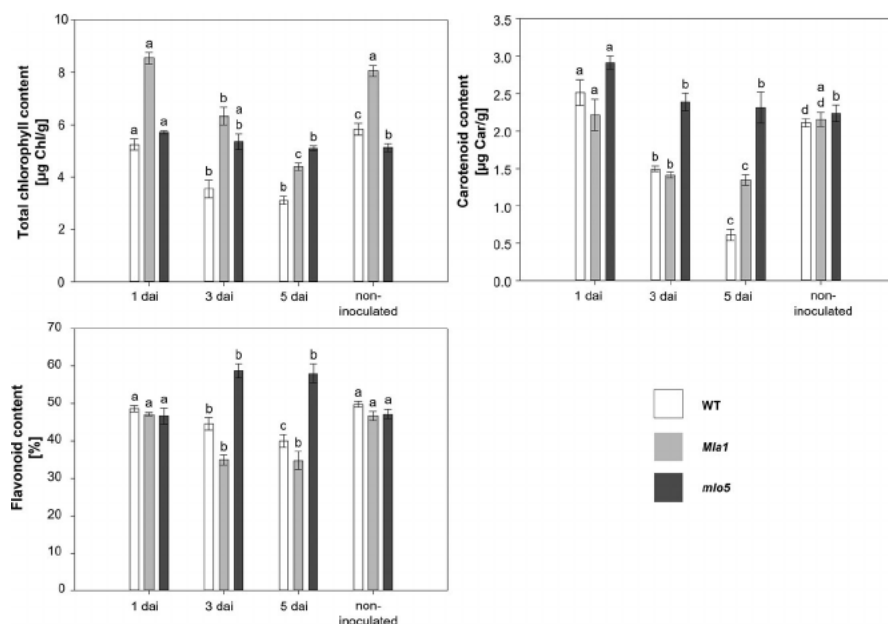
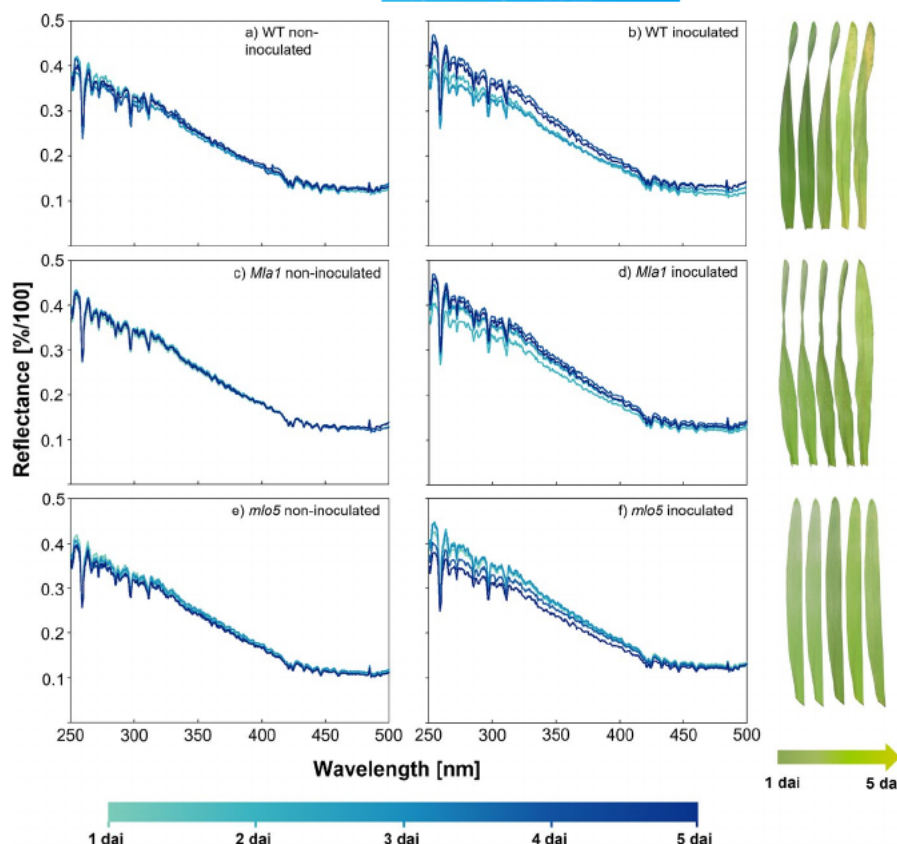


FIGURE 2 Pigment and flavonoid analysis of susceptible and resistant barley-*Blumeria graminis* f. sp. *hordei* (Bgh) interactions. Total chlorophyll, carotenoid and flavonoid extraction of noninoculated barley leaves and barley leaves inoculated with Bgh of Ingrid wild type (WT), *Mla1*, and *mlo5*. Analysis was performed 1, 3, and 5 days after inoculation (dai) and standard deviation is indicated. Lower case letters stand for significant difference between dai per genotype for which data was tested with Kolmogorov-Smirnov test for normal distribution with $p \leq 0.05$ and a Tukey's range test was applied with $\alpha = 0.05$

FIGURE 3 Spectral signatures of noninoculated and inoculated barley leaves and RGB visualization. Spectral signatures of noninoculated barley leaves (a,c,e) and barley leaves inoculated with *Blumeria graminis* f. sp. *hordei* (Bgh) (b,d,f). Ingrid wild type (WT), *Mla1*, and *mlo5* were used and incubated on phytoagar. RGB images of inoculated leaves 1 to 5 days after inoculation (dai) are displayed on the right [Colour figure can be viewed at wileyonlinelibrary.com]



measurements was homogeneous from 418 nm onward. The highest reflectance at 500 nm was measured at 5 dai at 0.145%. The broad-spectrum resistant genotype *mlo5* showed the highest reflectance of 0.44% at 254 nm 1 dai and decreased to 0.37% 5 dai. At 418 nm, all measurements displayed a similar reflectance except 5 dai, which was characterized by a smaller reflectance. From 460 nm onward, the reflectance of all measurements was similar and reached 0.1% at 500 nm.

All noninoculated leaves demonstrated constant spectral signatures, while inoculated WT leaves presented an overall decrease in reflectance up to 3 dai, before increasing and reaching the highest values 4 dai. Resistant *Mla1* leaves displayed an increase from 250 to 418 nm, increasing daily until the highest values were reached 5 dai. Resistant *mlo5* leaves decreased daily between 250 and 418 nm, and were represented by low values 5 dai.

3.4 | Classification of noninoculated and inoculated samples with deep learning

A neural network architecture with attention mechanism, so-called self-attention network (SAN) (Skrlić et al., 2020) was chosen as the classification method. Attention-based neural networks are a novel deep learning architecture which have achieved recent advances in various fields. However, they have not been considered as feature importance extractors for biological or hyperspectral data. The attention mechanism in the first layers of the network was used to classify particularly important elements of the feature space and

filter them out of the rest. Then, the classification layer used the parts identified as important to classify the input. Table 2 shows the achieved accuracy (average and standard deviation) of the SAN compared to the well-established gradient tree boosting (GB) method (Chen & Guestrin, 2016). SAN consistently achieved higher performances, with both methods having the highest accuracy at 1 and 5 dai. The WT genotype displayed values of 89% 5 dai, while *Mla1* and *mlo5* achieved 91% for the SAN method.

3.5 | Feature importance identifies relevant wavelengths

The self-attention block of the trained network was used to determine the feature importance. For this, the softmax-activated output of the self-attention block was extracted. Figure 6 visualizes the average over the cross-validated models. Only features with weighting above 5% are shown. In all three genotypes, 262 or 264 nm were identified as important wavelengths. For WT leaves, 263, 280, and 478 nm were also identified. For both resistant genotypes, 501 nm was additionally identified.

3.6 | Changes of secondary plant metabolites linked to relevant wavelengths

The wavelengths identified by feature importance are in the range from 262 to 291 nm and 442 to 500 nm. In both ranges, WT and

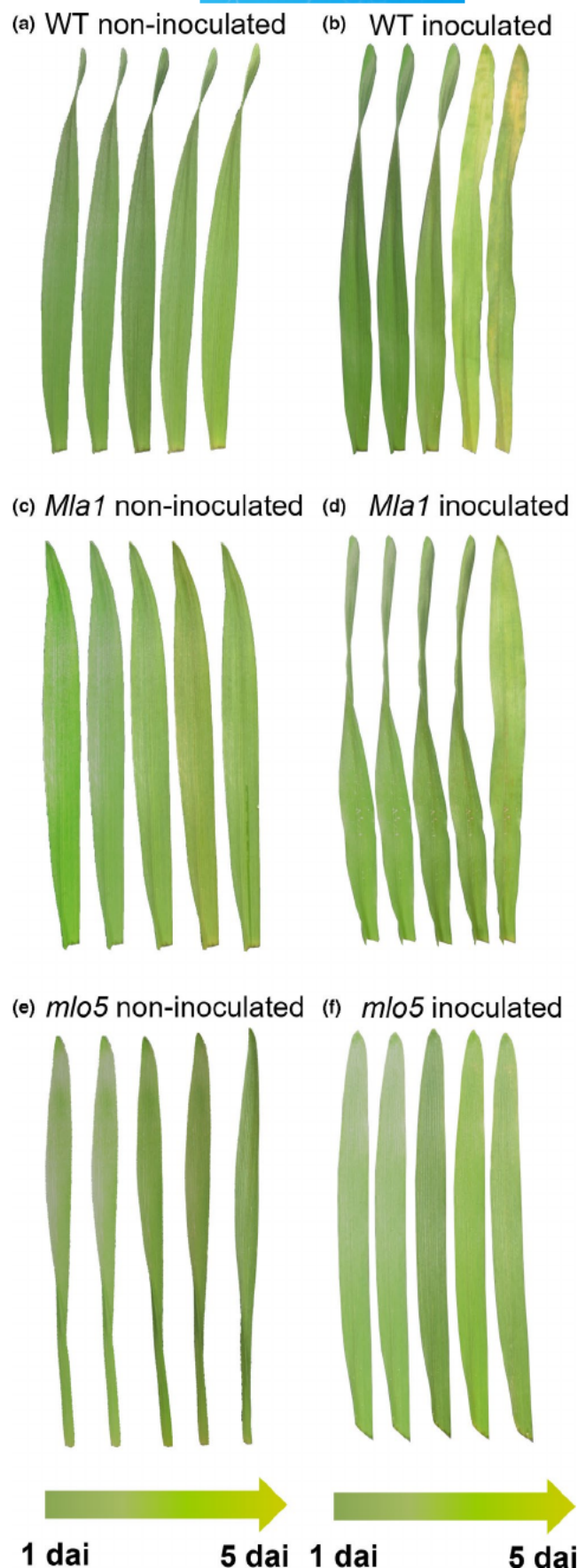


FIGURE 4 RGB images of noninoculated barley leaves and barley leaves inoculated with *Blumeria graminis* f. sp. *hordei* (Bgh) Ingrid wild type (WT), *Mla1*, and *mlo5* 1 to 5 days after inoculation (dai). Noninoculated leaves of all genotypes were healthy throughout, while inoculated leaves showed a typical resistant or susceptible reaction [Colour figure can be viewed at wileyonlinelibrary.com]

Mla1 leaves were represented by an increase of reflectance from 1 to 5 dai and showed a decrease in chlorophyll, carotenoid, and flavonoids. *mlo5* leaves displayed a decrease of reflectance in the range from 262 to 291 nm and an increase of flavonoids, but similar values of reflectance were recorded in the range from 442 to 500 nm from 1 to 5 dai, and extraction experiments showed a small decrease in chlorophyll and a constant value of carotenoid content.

4 | DISCUSSION

In this study, hyperspectral imaging in the UV range was used to investigate changes in secondary plant metabolites and pigments in susceptible and resistant barley powdery mildew interactions. The use of hyperspectral imaging to provide non-invasive information on host-pathogen interactions by assessing specific changes in plant reflectance patterns, which can be associated with physiological processes, has been well described (Mahlein et al., 2018; Thomas et al., 2018). Near-isogenic barley lines with different susceptibility towards Bgh have been previously studied with hyperspectral imaging and revealed different dynamics over time (Kuska et al., 2015, 2017). The first such studies connected multispectral imaging in the visible and near infrared range with the activity of invertase isoenzymes, and analysed the activity of cell wall, cytosolic, and vacuole invertase. Although this shows that multispectral imaging and invertase analysis complement each other, the correlation between hyperspectral imaging data and plant metabolites has not been previously studied. Therefore, this study of resistant and susceptible plant-pathogen response demonstrates the ability of UV hyperspectral imaging in combination with deep learning to identify changes in secondary plant metabolites.

The development of Bgh on WT leaves was as described (Both et al., 2005), and typical white pustules were visible 4 dai. Inoculated resistant leaves containing a *mlo* mutation showed no symptoms, as CWAs were formed at the penetration site, stopping further development (Jørgensen & Wolfe, 1994). Inoculated plants containing the resistant *Mla1* gene showed no symptoms, but from 4 dai brown necrotic spots were visible on the leaves. Once the penetration peg ruptures the cell wall and enters the epidermal cell, a race-specific resistance gene recognizes the Bgh avirulence factors and H_2O_2 is produced (Caldo et al., 2004). H_2O_2 triggers a HR and causes cell death of the penetrated epidermal cell, which is visible as brown, necrotic spots (Schulze-Lefert & Vogel, 2000).

The interaction of the sensor and illumination caused significant peaks from 250 to 321 nm and from 410 to 440 nm, which could not be removed by normalization. Therefore, a correlation of these wavelengths to specific secondary plant metabolites cannot be

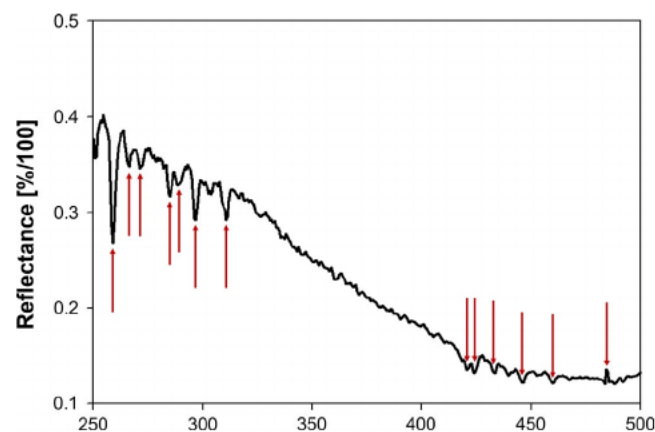


FIGURE 5 Visualization of relevant peaks due to the interaction of the sensor and illumination which were not considered in this investigation. Peaks are identified between 250 and 312 nm (258, 266, 271 nm) and between 410 and 440 nm (421, 423, 439 nm) [Colour figure can be viewed at wileyonlinelibrary.com]

TABLE 2 Cross-validated classification results of all three *Blumeria graminis* f. sp. *hordei* genotypes

Genotype	Days after inoculation	Gradient tree boosting (%)	Self-attention networks (%)
Wild type	1	84.73 ± 1.71	99.35 ± 0.75
	3	76.00 ± 1.39	79.69 ± 1.87
	5	84.31 ± 1.94	89.28 ± 0.82
<i>Mla1</i>	1	85.56 ± 1.51	96.10 ± 1.77
	3	75.99 ± 0.66	78.65 ± 1.54
	5	81.70 ± 0.81	91.69 ± 1.63
<i>mlo5</i>	1	83.62 ± 1.15	99.19 ± 0.51
	3	74.99 ± 2.28	82.12 ± 2.48
	5	84.34 ± 2.22	91.09 ± 2.35

Note: Data are mean ± SD. The accuracy of self-attention networks is shown in comparison to the established gradient tree boosting method.

verified. Untreated barley leaves showed no changes in spectral signatures and no senescence during the observation period, which corresponds to the phenotypic development of barley leaves (Figure 3). The increase in reflectance of inoculated WT leaves from 450 nm onward can be linked to a decrease in plant pigments such as chlorophyll and carotenoids (Brugger et al., 2018; Scholes et al., 1994) and is also reflected in the pigment analysis. Previous studies showed that 1 dai, susceptible WT leaves already showed a reduced photosynthetic performance due to reduced pigment content in the leaves (Brugger et al., 2018). Like WT, *Mla1* leaves showed an increase in reflectance from 450 to 500 nm 2 dai and a corresponding decrease in chlorophyll and carotenoid content. *Mla* resistance leads to a deterioration of photosynthesis and pigment metabolism, as HR causes necrosis (Matile et al., 1999). Previous studies with hyperspectral imaging showed that a reduction of plant pigments can already be detected 2 dai on *Mla1* leaves (Kuska et al., 2017), confirming the results in the UV range. Infected *mlo5* leaves showed no changes in

reflectance at 450–500 nm and an almost constant pigment content. Due to the formation of CWA, *mlo* resistant leaves are known for only small decreases in photosynthetic activity (Scholes & Rolfe, 2009) resulting in a high pigment content. Compared to *mlo5*, WT and *Mla1* leaves exhibited a faster senescence, visible as an increase in reflectance, while *mlo* leaves are known to display a delay in senescence and greening effect after inoculation (Kuska et al., 2015).

During the pathogenesis, reflectance increased in WT leaves from 250 to 370 nm, which can be associated with a decrease in flavonoids, because their absorption maxima are in the range of 240–290 nm and 320–370 nm (Mierziak et al., 2014). The flavonoid content of WT leaves slightly decreased, presumably because flavonoids act as catalysts in photosynthesis, which is downregulated in Bgh infections, resulting in a reduced need for flavonoids and subsequent downregulation of the flavonoid metabolism. In addition, flavonoids are categorized into preformed and induced compounds, whereby preformed flavonoids are produced during normal plant development and stored at important sites, for example, in epidermal cells. There they can play a direct role in the defence of pathogens or act as signalling compounds (Treutter, 2005). For this reason, a decrease in flavonoids in susceptible barley leaves after Bgh infection is plausible and evident both in the recorded spectral reflectance and in the analysis. An influence of the UV radiation on the leaves can be excluded, as this would have led to higher levels of flavonoids due to their protective function against UV light (Monici et al., 1993). *Mla1* leaves displayed a decrease in flavonoids from 1 to 3 dai before exhibiting constant values until 5 dai. Phenolic compounds, to which the group of flavonoids belongs, are stored in epidermal cells and, particularly in the case of HR and associated cell death, are released rapidly in infested tissue (Beckman, 2000). As this occurs in a *Mla1*-based resistance, the decrease in flavonoids in inoculated *Mla1* leaves can thus be explained. In addition, a previous study suggested that the release of flavonoids occurs particularly in early stages of infection (Beckman 2000), explaining the strong decrease of flavonoids from 1 to 3 dai in the present study. In contrast to inoculated WT and *Mla1* leaves, *mlo5* leaves featured a decrease of reflectance from 250–370 nm during time-series measurements, corresponding to a strong increase of flavonoids 3 dai. Flavonoids are involved in auxin metabolism, which causes a tightening of the plant structure (Mierziak et al., 2014). This leads to the formation of callose and cell wall phenolics (von Roepenack et al., 1998), explaining the increase in flavonoids 3 dai. Additionally, studies with barley and *Fusarium* head blight revealed an accumulation of flavonoid glycosides as a resistance response against the fungi to strengthen cell walls and limit the infection (Karre et al., 2019). Similar patterns between WT and *Mla1* leaves can be explained by the previously mentioned early senescence after inoculation, while *mlo5* leaves displayed a characteristic delay in senescence. The analysis of flavonoids and pigments reflected the spectral signatures of each genotype, allowing a connection between the two to be established.

In this work, neural networks with self-attention mechanisms were used for the classification of healthy and diseased plants, identifying the most relevant parts of the input for this task. Due to the decreasing costs of cameras, hyperspectral imaging becomes more

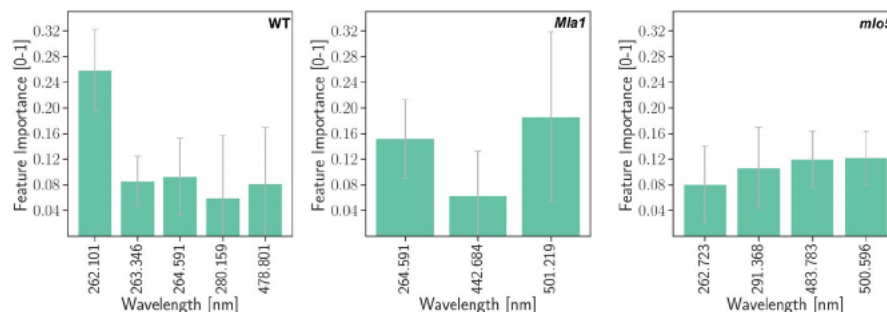


FIGURE 6 Resulting feature importance of the classification network to differentiate between inoculated and noninoculated data of the *Blumeria graminis* f. sp. *hordei* (Bgh) genotypes wild type (WT), *Mla1*, and *mlo5*. For each genotype, wavelengths with a weighting of more than 5% are highlighted and standard deviation is indicated. Wavelengths from 262 to 291 nm were connected with flavonoids, and from 442 to 500 nm with chlorophyll and carotenoids [Colour figure can be viewed at wileyonlinelibrary.com]

and more popular, and researchers and developers have better access to this technology (Mahlein et al., 2019). Because hyperspectral imaging leads to large amounts of data, deep learning methods have been used to identify plant diseases, such as the use of deep convolutional neural networks to identify charcoal rot disease in soybean stems (Nagasubramanian et al., 2019) and other applications (Polder et al., 2019; Schramowski et al. 2020; Tetila et al., 2019).

Data mining methods have also been used to localize HR from hyperspectral imaging data before they were visible on RGB images (Kuska et al., 2017). Singh et al., (2018) reviewed the trends and future perspectives of using deep learning techniques for plant stress phenotyping, and stated the great promise for improving speed, accuracy, reliability, and scalability of disease phenotyping. The classification of noninoculated and inoculated samples with deep learning revealed that SAN consistently achieved higher performance compared to GB. This aligns with previous findings that applying SAN results in an improved performance on data sets with many features (Skrlić et al., 2020). The classification performance and feature importance identification were cross-validated using SANs and the results were verified by biological investigation. However, different feature importance estimation approaches for deep neural networks, for instance attribution methods such as LIME (Riberio et al., 2016) and saliency maps (Karen et al., 2014), could result in slightly deviating importances. Further, the estimation also depends on the general performance of the underlying model. However, one of the advantages of SAN is that the feature importance is computed during inference, and does not rely on an external linear approximate of the deep learning model, such as used in LIME (Riberio et al., 2016). Nevertheless, future work should address different kinds of deep feature importance extractors and analyse their differences.

It is striking that both SAN and GB have the highest accuracy at 1 and 5 dai. The high accuracy at 1 dai can be explained by the inoculation methodology, because the samples were inoculated by using a brush to apply the Bgh spores on the leaves immediately before the first measurement. While noninoculated leaves were treated with a clean brush, fresh spores covered the surface of inoculated leaves and therefore changed the optical properties of the plant, which eased the classification. High classification accuracy 5 dai are linked to visible symptoms on WT and *Mla1* leaves and noticeable

higher reflectance of *mlo5* leaves. The feature importance identified 264 nm as the most important wavelength for the classification of all three genotypes, and because flavonoids feature an absorption maximum at 240–290 nm (Mierziak et al., 2014), this wavelength can be linked to flavonoids. Other wavelengths with lesser feature importance value were identified at 442 and 478 nm. These wavelengths were linked to a change in pigments including chlorophyll and carotenoids, which feature absorption maxima from 400–500 nm (Lichtenthaler, 1987).

Secondary plant metabolites which can be linked by feature importance to identified wavelengths showed changes in content in extraction experiments that were also consistent with the spectra recorded in the UV range. This information can be used to characterize different host-pathogen interactions, as they lead to differences in secondary plant metabolites, which are reflected in changes in reflectance. Thus, hyperspectral imaging in the UV range could lead to information about changes in secondary plant metabolites such as chlorophyll, carotenoid, and flavonoids, depending on susceptibility or resistance reactions.

This study showed that spectral information in the UV range of different host-pathogen interactions corresponds to changes in secondary plant metabolites. Specific resistance responses in incompatible barley-Bgh interactions can also be differentiated by spectral reflectance. In addition, deep learning revealed that these secondary plant metabolites can be linked to wavelengths which are of importance for the classification of healthy and diseased plants. Therefore, hyperspectral imaging in the UV range and deep learning can provide an understanding of susceptible and resistant responses of plants and can be used as a nondestructive tool to achieve a greater knowledge about plant-pathogen interactions.

ACKNOWLEDGEMENTS

The authors are thankful to Jan Behmann, Marcus Jansen, and Hans-Georg Luigs for support on technical issues and Sabine von Tiedemann for proofreading and helpful comments on the manuscript. The project is supported by funds of the German Federal Ministry of Food and Agriculture (BMEL) based on a decision of the Parliament of the Federal Republic of Germany via the Federal Office for Agriculture and Food (BLE) under the innovation support program,

project “DePhenSe” (FKZ 2818204715) and was partially funded by the Deutsche Forschungsgemeinschaft (DFG, German Research Foundation) under Germany's Excellence Strategy – EXC 2070 – 390732324. The authors declare that they have no competing interests. Open Access funding enabled and organized by Projekt DEAL.

DATA AVAILABILITY STATEMENT

The data that support the findings of this study are available from the corresponding author upon reasonable request.

ORCID

Anna Brugger  <https://orcid.org/0000-0003-3360-345X>

REFERENCES

- Abu-Eittah, R.H. & El-Tawil, B.A.H. (1985) The electronic absorption spectra of some coumarins. A molecular orbital treatment. *Canadian Journal of Chemistry*, **63**, 1173–1179.
- Beckman, C.H. (2000) Phenolic-storing cells: keys to programmed cell death and periderm formation in wilt disease resistance and in general defence responses in plants? *Physiological and Molecular Plant Pathology*, **57**, 101–110.
- Both, M., Csukai, M., Stumpf, M.P. & Spanu, P.D. (2005) Gene expression profiles of *Blumeria graminis* indicate dynamic changes to primary metabolism during development of an obligate biotrophic pathogen. *The Plant Cell*, **17**, 2107–2122.
- Brugger, A., Behmann, J., Paulus, S., Luigs, H.-G., Kuska, M.T., Schramowski, P. et al (2019) Extending hyperspectral imaging for plant phenotyping to the UV range. *Remote Sensing*, **11**, 1401. <https://doi.org/10.3390/rs11121401>
- Brugger, A., Kuska, M.T. & Mahlein, A.-K. (2018) Impact of compatible and incompatible barley - *Blumeria graminis* f.sp. *hordei* interactions on chlorophyll fluorescence parameters. *Journal of Plant Diseases and Protection*, **125**, 177–186.
- Caldo, R.A., Nettleton, D. & Wise, R.P. (2004) Interaction-dependent gene expression in mla-specified response to barley powdery mildew. *The Plant Cell*, **16**, 2514–2528.
- Chen, T. & Guestrin, C. (2016) Xgboost: A scalable tree boosting system. *arXiv*, 1603.02754. [Preprint].
- Devlin, J., Chang, M.-W., Lee, K. & Toutanova, K. (2018) Bert: Pre-training of deep bidirectional transformers for language understanding. *arXiv*, 1810.04805. [Preprint].
- Hiscox, J. & Israelstam, G. (1979) A method for the extraction of chlorophyll from leaf tissue without maceration. *Canadian Journal of Botany*, **57**, 1332–1334. <https://doi.org/10.1139/b79-163>
- Jørgensen, I.H. (1992) Discovery, characterization and exploitation of mlo powdery mildew resistance in barley. *Euphytica*, **63**, 141–152. <https://doi.org/10.1007/BF00023919>
- Jørgensen, J.H. & Wolfe, M. (1994) Genetics of powdery mildew resistance in barley. *Critical Reviews in Plant Sciences*, **13**, 97–119. <https://doi.org/10.1080/07352689409701910>
- Karen, S., Andrea, V. & Andrew, Z. (2014) Deep inside convolutional networks: visualising image classification models and saliency maps. In: *Workshop Track Proceedings of 2nd International Conference on Learning Representations*. Available at: <https://arxiv.org/abs/1312.6034> [Accessed 12 May 2021].
- Karre, S., Kumar, A., Yogendra, K., Kage, U., Kushalappa, A. & Charron, J.-B. (2019) Hvwrky23 regulates flavonoid glycoside and hydroxycinnamic acid amide biosynthetic genes in barley to combat fusarium head blight. *Plant Molecular Biology*, **100**, 591–605. <https://doi.org/10.1007/s11103-019-00882-2>
- Kingma, D.P. & Ba, J. (2014) Adam: A method for stochastic optimization. *arXiv*, 1412.6980. [Preprint].
- Klambauer, G., Unterthiner, T., Mayr, A. & Hochreiter, S. (2017) Self-normalizing neural networks. In: Guyon, I., von Luxburg, U., Bengio, S., Wallach, H.M., Fergus, R., Vishwanathan, S.V.N. & Garnett, R. (Eds.) *Advances in Neural Information Processing Systems* **30**, 971–980.
- Kølster, P., Munk, L., Stølen, O. & Løhde, J. (1986) Near-isogenic barley lines with genes for resistance to powdery mildew. *Crop Science*, **26**, 903–907.
- Kuska, M.T., Behmann, J., Großkinsky, D.K., Roitsch, T. & Mahlein, A.-K. (2018) Screening of barley resistance against powdery mildew by simultaneous high-throughput enzyme activity signature profiling and multispectral imaging. *Frontiers in Plant Science*, **9**, 1074. <https://doi.org/10.3389/fpls.2018.01074>
- Kuska, M.T., Brugger, A., Thomas, S., Wahabzada, M., Kersting, K., Oerke, E.-C. et al (2017) Spectral patterns reveal early resistance reactions of barley against *Blumeria graminis* f. sp. *hordei*. *Phytopathology*, **107**, 1388–1398.
- Kuska, M., Wahabzada, M., Leucker, M., Dehne, H.-W., Kersting, K., Oerke, E.-C. et al (2015) Hyperspectral phenotyping on the microscopic scale: towards automated characterization of plant-pathogen interactions. *Plant Methods*, **11**, article 28.
- Lichtenthaler, H. (1987) Chlorophyll and carotenoids-pigments of photosynthetic biomembranes. *Methods in Enzymology*, **148**, 350–382.
- Lichtenthaler, H.K. & Buschmann, C. (2001) Chlorophylls and carotenoids: Measurement and characterization by UV-VIS spectroscopy. *Current Protocols in Food Analytical Chemistry*, F4.3.1–F4.3.8.
- Liu, L., Gitz, D.C. & McClure, J.W. (1995) Effects of UV-b on flavonoids, ferulic acid, growth and photosynthesis in barley primary leaves. *Physiologia Plantarum*, **93**, 725–733. <https://doi.org/10.1111/j.1399-3054.1995.tb05123.x>
- Liu, Z.-H., Kanjo, Y. & Mizutani, S. (2010) A review of phytoestrogens: their occurrence and fate in the environment. *Water Research*, **44**, 567–577. <https://doi.org/10.1016/j.watres.2009.03.025>
- Madden, H.H. (1978) Comments on the savitzky-golay convolution method for least-squares-fit smoothing and differentiation of digital data. *Analytical Chemistry*, **50**, 1383–1386. <https://doi.org/10.1021/ac50031a048>
- Mahlein, A.-K., Kuska, M.T., Behmann, J., Polder, G. & Walter, A. (2018) Hyperspectral sensors and imaging technologies in phytopathology: state of the art. *Annual Review of Phytopathology*, **56**, 535–558. <https://doi.org/10.1146/annurev-phyto-080417-050100>
- Mahlein, A.-K., Kuska, M.T., Thomas, S., Wahabzada, M., Behmann, J., Rascher, U. et al (2019) Quantitative and qualitative phenotyping of disease resistance of crops by hyperspectral sensors: seamless interlocking of phytopathology, sensors, and machine learning is needed!. *Current Opinion in Plant Biology*, **50**, 156–162. <https://doi.org/10.1016/j.pbi.2019.06.007>
- Matile, P., Hörtensteiner, S. & Thomas, H. (1999) Chlorophyll degradation. *Annual Review of Plant Biology*, **50**, 67–95. <https://doi.org/10.1146/annurev.arplant.50.1.67>
- Mierziak, J., Kostyn, K. & Kulma, A. (2014) Flavonoids as important molecules of plant interactions with the environment. *Molecules*, **19**, 16240–16265. <https://doi.org/10.3390/molecules191016240>
- Mihai, C.M., Mărghițaș, L.A., Bobiș, O., Dezmiorean, D. & Tamaș, M. (2010) Estimation of flavonoid content in propolis by two different colorimetric methods. *Scientific Papers: Animal Science and Biotechnologies*, **43**, 407–410.
- Monici, M., Baglioni, P., Mulinacci, N., Baldi, A. & Vincieri, F.F. (1993) A research model on flavonoids as photoprotectors: studies on the photochemistry of kaempferol and pelargonidin. *International Symposium on Natural Phenols in Plant Resistance*, **381**, 340–347.
- Nagasubramanian, K., Jones, S., Singh, A.K., Sarkar, S., Singh, A. & Ganapathysubramanian, B. (2019) Plant disease identification using explainable 3D deep learning on hyperspectral images. *Plant Methods*, **15**, 98. <https://doi.org/10.1186/s13007-019-0479-8>

- Neil, S.O. & Gould, K.S. (2003) Anthocyanins in leaves: light attenuators or antioxidants? *Functional Plant Biology*, 30, 865–873. <https://doi.org/10.1071/FP03118>
- Petrussa, E., Braidot, E., Zancani, M., Peresson, C., Bertolini, A., Patui, S. et al (2013) Plant flavonoids—biosynthesis, transport and involvement in stress responses. *International Journal of Molecular Sciences*, 14, 14950–14973. <https://doi.org/10.3390/ijms140714950>
- Polder, G., Blok, P., De Villiers, H., Wolf, J. & Kamp, J. (2019) Potato virus Y detection in seed potatoes using deep learning on hyperspectral images. *Frontiers in Plant Science*, 10, 209. <https://doi.org/10.3389/fpls.2019.00209>
- Reiser, A., Leyshon, L., Saunders, D., Mijovic, M., Bright, A. & Bogie, J. (1972) Fluorescence of aromatic benzoxazole derivatives. *Journal of the American Chemical Society*, 94, 2414–2421. <https://doi.org/10.1021/ja00762a036>
- Ribeiro, M.T., Singh, S. & Guestrin, C. (2016) "Why should I trust you?": Explaining the predictions of any classifier., *arXiv*, 1602.04938. [Preprint].
- Scholes, J., Lee, P., Horton, P. & Lewis, D. (1994) Invertase: understanding changes in the photosynthetic and carbohydrate metabolism of barley leaves infected with powdery mildew. *New Phytologist*, 126, 213–222. <https://doi.org/10.1111/j.1469-8137.1994.tb03939.x>
- Scholes, J.D. & Rolfe, S.A. (2009) Chlorophyll fluorescence imaging as tool for understanding the impact of fungal diseases on plant performance: a phenomics perspective. *Functional Plant Biology*, 36, 880–892. <https://doi.org/10.1071/FP09145>
- Schramowski, P., Stammer, W., Teso, S., Brugger, A., Herbert, F., Shao, X. et al (2020) Making deep neural networks right for the right scientific reasons by interacting with their explanations. *Nature Machine Intelligence*, 2, 476–486. <https://doi.org/10.1038/s42256-020-0212-3>
- Schulze-Lefert, P. & Vogel, J. (2000) Closing the ranks to attack by powdery mildew. *Trends in Plant Science*, 5, 343–348. [https://doi.org/10.1016/S1360-1385\(00\)01683-6](https://doi.org/10.1016/S1360-1385(00)01683-6)
- Seely, G. & Jensen, R. (1965) Effect of solvent on the spectrum of chlorophyll. *Spectrochimica Acta*, 21, 1835–1845. [https://doi.org/10.1016/0371-1951\(65\)80095-9](https://doi.org/10.1016/0371-1951(65)80095-9)
- Singh, A.K., Ganapathysubramanian, B., Sarkar, S. & Singh, A. (2018) Deep learning for plant stress phenotyping: trends and future perspectives. *Trends in Plant Science*, 23, 883–898. <https://doi.org/10.1016/j.tplants.2018.07.004>
- Skrli, B., Dzeroski, S., Lavrac, N. & Petkovic, M. (2020) Feature importance estimation with self-attention networks. *arXiv*, 2002.04464. [Preprint].
- Snyder, R. & Testa, A. (1984) Influence of electron-donor- acceptor complexation on electronic relaxation of quinoline. *Journal of Physical Chemistry*, 88, 5948–5950. <https://doi.org/10.1021/j150668a040>
- Stalin, T., Devi, R.A. & Rajendiran, N. (2005) Spectral characteristics of ortho, meta and para dihydroxy benzenes indifferent solvents, pH and β -cyclodextrin. *Spectrochimica Acta Part A: Molecular and Biomolecular Spectroscopy*, 61, 2495–2504. <https://doi.org/10.1016/j.saa.2004.08.024>
- Taniguchi, M. & Lindsey, J.S. (2018) Database of absorption and fluorescence spectra of >300 common compounds for use in PhotochemCAD. *Photochemistry and Photobiology*, 94, 290–327.
- Tetila, E.C., Machado, B.B., Menezes, G.K., Da Silva Oliveira, A., Alvarez, M., Amorim, W.P. et al (2019) Automatic recognition of soybean leaf diseases using UAV images and deep convolutional neural networks. *IEEE Geoscience and Remote Sensing Letters*, 17, 903–907. <https://doi.org/10.1109/LGRS.2019.2932385>
- Thomas, S., Kuska, M.T., Bohnenkamp, D., Brugger, A., Alisaac, E., Wahabzada, M. et al (2018) Benefits of hyperspectral imaging for plant disease detection and plant protection: a technical perspective. *Journal of Plant Diseases and Protection*, 125, 5–20. <https://doi.org/10.1007/s41348-017-0124-6>
- Thomas, S., Wahabzada, M., Kuska, M.T., Rascher, U. & Mahlein, A.-K. (2016) Observation of plant-pathogen interaction by simultaneous hyperspectral imaging reflection and transmission measurements. *Functional Plant Biology*, 44, 23–34. <https://doi.org/10.1071/FP16127>
- Treutter, D. (2005) Significance of flavonoids in plant resistance and enhancement of their biosynthesis. *Plant Biology*, 7, 581–591. <https://doi.org/10.1055/s-2005-873009>
- Treutter, D. (2006) Significance of flavonoids in plant resistance: a review. *Environmental Chemistry Letters*, 4, 147. <https://doi.org/10.1007/s10311-006-0068-8>
- Vaswani, A., Shazeer, N., Parmar, N., Uszkoreit, J., Jones, L., Gomez, A.N. et al (2017) Attention is all you need. *Advances in Neural Information Processing Systems*, 5998–6008.
- von Roepenack, E., Parr, A. & Schulze-Lefert, P. (1998) Structural analyses and dynamics of soluble and cellwall-bound phenolics in a broad spectrum resistance to the powdery mildew fungus in barley. *Journal of Biological Chemistry*, 273, 9013–9022. <https://doi.org/10.1074/jbc.273.15.9013>
- Witzenberger, A., Hack, H. & Van Den Boom, T. (1989) Erläuterungen zum BBCH-Dezimal-Code für die Entwicklungsstadien des Getreides – mit Abbildungen. *Gesunde Pflanzen*, 41, 384–388.
- Woodall, G. & Stewart, G. (1998) Do anthocyanins play a role in UV protection of the red juvenile leaves of syzygium? *Journal of Experimental Botany*, 49, 1447–1450. <https://doi.org/10.1093/jxb/49.325.1447>

How to cite this article: Brugger, A., Schramowski, P., Paulus, S., Steiner, U., Kersting, K. & Mahlein, A.-K. (2021) Spectral signatures in the UV range can be combined with secondary plant metabolites by deep learning to characterize barley–powdery mildew interaction. *Plant Pathology*, 70, 1572–1582. <https://doi.org/10.1111/ppa.13411>